Radio observations of the fine structure inside a post-CME current sheet *

Guan-Nan Gao[1,2,3], Min Wang[1,3,4], Jun Lin[1], Ning Wu[5], Cheng-Ming Tan[4],
Berhard Kliem[1,6] and Yang Su[7]

[1] Yunnan Observatories, Chinese Academy of Sciences, Kunming 650011, China;
   ggn@ynao.ac.cn
[2] University of Chinese Academy of Sciences, Beijing 100049, China
[3] Key Laboratory for the Structure and Evolution of Celestial Objects, Yunnan Observatories,
   Chinese Academy of Sciences, Kunming 650011, China
[4] Key Laboratory of Solar Activity, National Astronomical Observatories, Chinese Academy of
   Sciences, Beijing 100012, China
[5] School of Tourism and Geography, Yunnan Normal University, Kunming 650031, China
[6] Institute of Physics and Astronomy, University of Potsdam, Potsdam 14476, Germany
[7] IGAM-Kanzelhöhe Observatory, Institute of Physics, University of Graz, Universitätsplatz 5,
   8010 Graz, Austria

Abstract   A solar radio burst was observed in a coronal mass ejection/flare event by
the Solar Broadband Radio Spectrometer at the Huairou Solar Observing Station on
2004 December 1. The data exhibited various patterns of plasma motions, suggestive
of the interaction between sunward moving plasmoids and the flare loop system during
the impulsive phase of the event. In addition to the radio data, the associated white-
light, Hα, extreme ultraviolet light, and soft and hard X-rays were also studied.

Key words: Sun: coronal mass ejections (CMEs)— Sun: flares — Sun: solar radio
bursts — Sun: magnetic reconnection

1 INTRODUCTION

Long current sheets always develop between coronal mass ejections (CMEs) and the associated
flares in major solar eruptions as the closed coronal magnetic field is severely stretched (Fig. 1, and
see Lin & Forbes 2000; Lin et al. 2003). Magnetic reconnection occurring inside the sheet due to
various plasma instabilities and turbulence plays a fundamental role in converting magnetic energy
into heat and kinetic energy of the plasma during the eruption. In this process, various phenomena
occur and are visible in the current sheet. These manifestations are either related to the causes of
the reconnection itself, or produced by reconnection. The former includes plasma blobs flowing in
the sheet (Ko et al. 2003; Lin et al. 2005; Savage et al. 2010; and references therein), and the latter
includes the growing flare loop system, the termination shock (TS) on top of the flare loop as a result
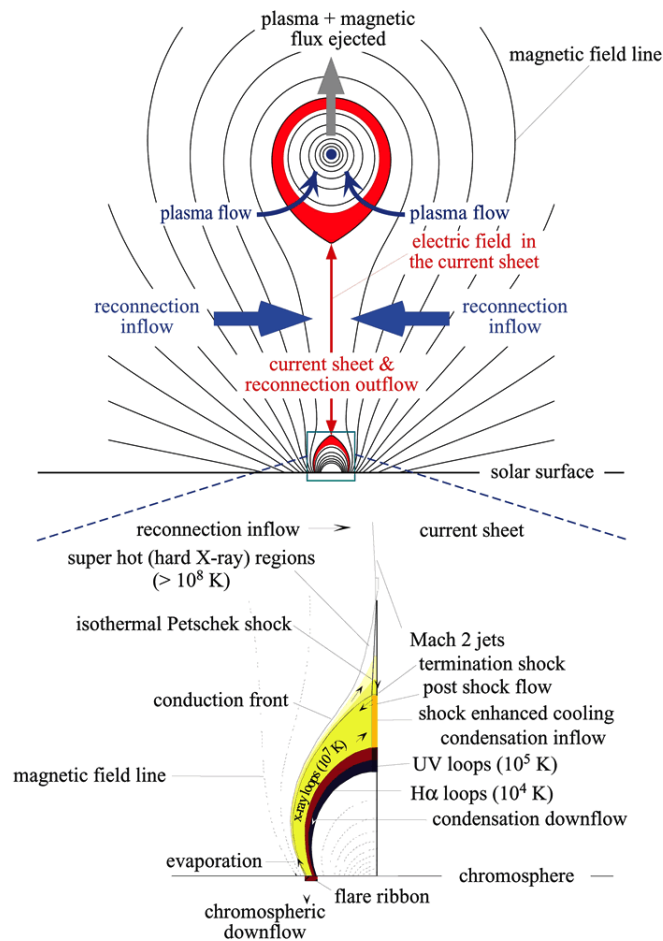of the interaction between sunward moving plasma blobs and the closed flare loops, as well as the

---

Fig. 1 Schematic diagram of the Lin-Forbes CME-Flare model. Colors are used to indicate the plasma layers at different temperatures. This diagram incorporates the two-ribbon flare configurations of Forbes & Acton (1996) and the CME configuration of Lin & Forbes (2000). This model clearly marks the position of the TS and the downward reconnection outflow.

shrinkage of individual loops as soon as they are created by reconnection (e.g. see also Forbes & Acton 1996; Lin 2004; Huang & Lin 2006; Yan et al. 2013; and references therein).

Evidence of the above features was also reported in both radio and hard X-ray emissions. The drifting pulsating structures displayed in the dynamic spectra of the decimetric band are believed to be representative of the plasmoid motion in the current sheet (e.g. see Kliem et al. 2000; Karlický & Bárta 2012; and references therein). Although it is not difficult to understand that the TS could result from the interaction of the reconnection outflow with the closed flare loops, it has proven very difficult, if not impossible, to observe or recognize the TS.

So far, only two events have been reported that display signatures of the TS by Aurass et al. (2002) and Aurass & Mann (2004). In the first case, a zero-drift type II-like radio burst was detected in the frequency range from 300 to 400 MHz in the late phase of the flare; and in the second case, two zero-drift type II-like bursts were observed in the metric ($\sim$300 MHz) and decimetric (30$-$80 MHz)

(a) C2 2004/12/01 08:06:05
(b) C2 2004/12/01 08:29:57
(C) C3 2004/12/01 08:42:29
(d) C3 2004/12/01 09:18:05
(E) C3 2004/12/01 09:42:06
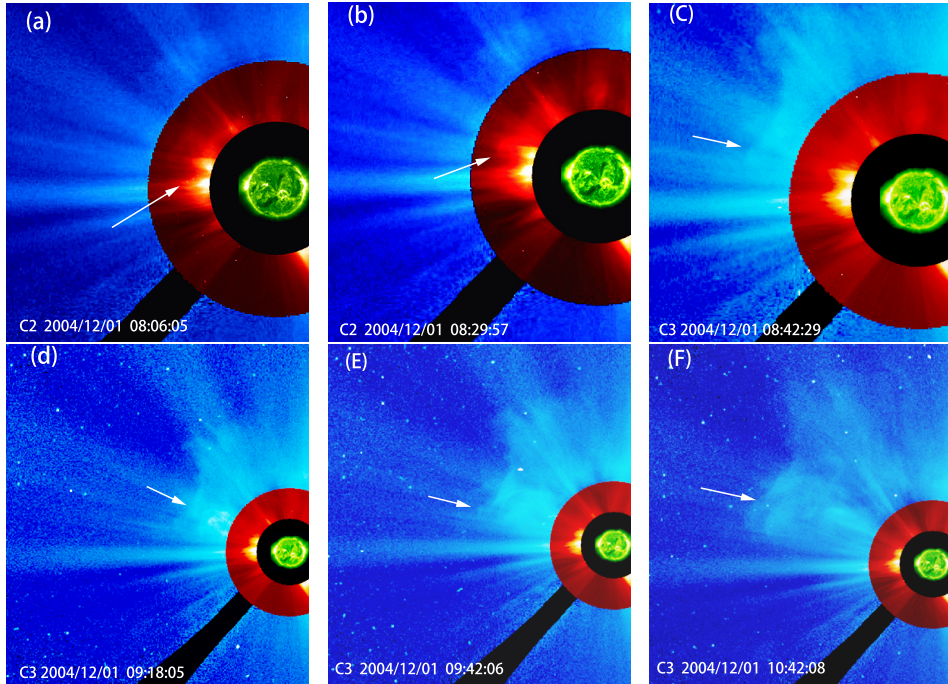(F) C3 2004/12/01 10:42:08

Fig. 2 Composite EIT-LASCO/C2-C3 images of the CME at different times; the arrow in each panel specifies the CME front.

bands, respectively. The emission in the decimetric band, on the other hand, was explained as the result of the interaction of the anti-sunward reconnection outflow with the bottom of the CME bubble (see also discussions of Lin et al. 2004 and Lin & Soon 2004). Furthermore, an X-17 flare on 2003 October 28 showed a slowly drifting type II-like emission, which was interpreted as being due to the TS of the sunward reconnection outflow (Mann et al. 2006).

In this work, we study a solar radio burst observed by the Solar Broadband Radio Spectrometer (SBRS) (Fu et al. 1995, 2004) at the Huairou Solar Observing Station (HSOS) in a CME/flare event on 2004 December 1. This event produced a CME with a speed of $\sim$800 km s^{-1} from the North-East limb (see Fig. 2) and an M 1.1 flare according to the GOES data (see Fig. 3). The radio burst was detected at frequencies slightly above 1 GHz and showed complex fine structures consisting of narrow-band emission stripes.

These fine structures have been interpreted in Ning et al. (2009) as evidence of precipitating electron beams and associated chromospheric evaporation, as first suggested in Aschwanden & Benz (1995). However, the temporal association of the radio stripes with the signatures of chromospheric evaporation in the hard X-ray data is very poor. Such signatures existed before and after the radio burst, but not simultaneously with it (see also Ning et al. 2009).

In the sections below, we will put forward a new explanation for this radio burst, which may also explain the related details displayed by the RHESSI data. We suggest that the radio burst reveals information about the plasmoids flowing in the current sheet and the interaction with the flare loop, as well as the motion of the flare loop system.

Section 2 describes the radio burst and the associated data in the white light, Hα, extreme ultra-violet light, soft and hard X-rays. Section 3 gives the data analysis for the radio dynamic spectrum
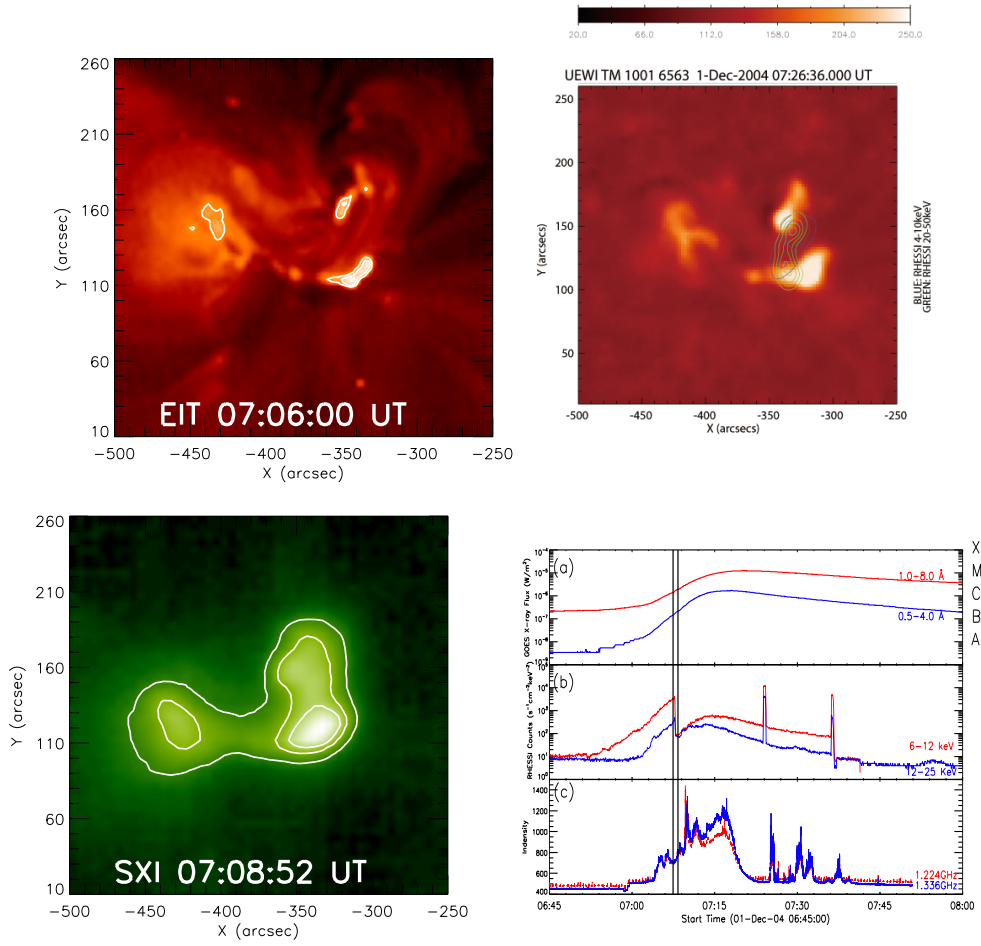
Fig. 3 *Upper left panel*: The EIT 284 Å image from the SOHO/EIT; *Upper right panel*: The Hα image observed by Kanzelhöhe Observatory overlayed with RHESSI data at the energy of 4–10 keV (*blue contours*) and of 20–50 keV (*green contours*); *Bottom left panel*: The SXR image from the SXI onboard the GOES-12 satellite. *Bottom right panel*: (a) the time profile of SXR flux from GOES, (b) the RHESSI light curves in two energy bands 6–12 keV and 12–25 keV, and (c) the radio profile curves in two frequencies 1.224 GHz and 1.336 GHz; the two vertical lines specify the time interval of radio bursts considered here.

and some interpretations of the radio burst. Section 4 gives some conclusions on the basis of the analysis of the above.

2 OBSERVATIONS

The CME in this event was first observed at 07:31:46 UT by the Large Angle Spectrometric Coronagraph (LASCO) (Brueckner et al. 1995) experiment onboard SOHO; it appeared in the field of view of LASCO/C2 at a speed of 834 km s^{-1} (see the LASCO CME Catalog: *http://cdaw. gsfc.nasa.gov/CME_list*).

Figure 2 displays a set of composites of EIT-LASCO/C2-C3 images of this CME. The arrow in each panel specifies the CME front.

Associated with the CME, an M 1.1 flare occurred in the active region AR 10708. It started at 07:00 UT and peaked at 07:20 UT. Figure 3 shows the 284 Å extreme ultraviolet (EUV) image (upper left panel) obtained by the EUV Imaging Telescope (EIT) onboard SOHO (Delaboudinière et al. 1995) and the soft X-ray (SXR) image (bottom left panel) by the Solar X-Ray Imager (SXI) onboard the GOES-12 satellite (Hill et al. 2005), both selected to be closest in time to the radio burst. The EUV image displays the flare ribbons and the SXR image shows cospatial footpoint sources of the flare loop on the right-hand side ($x \approx -350''$). The Hα image of interest that was obtained by the Kanzelhöhe Observatory is displayed in the upper right panel of Figure 3 overlapped with the data from RHESSI (Lin et al. 2002) at an energy of 4–10 keV (blue contours) and of 20–50 keV (green contours). The time profile of the SXR flux from GOES, radio data from HSOS and the RHESSI data are displayed in the bottom right panel of Figure 3, with the time interval of the radio burst we studied specified by the two vertical lines (see Fig. 3).

A secondary enhancement in the elongated southern flare ribbon at $x \approx -440''$ appears as an additional source in the SXI image. At this early stage of the flare's impulsive phase, the first group of flare loops between the two bright EUV and SXR sources is only faintly indicated. The Hα image shows an elongated southern flare ribbon similar to that in the EUV image. It also displays that a filament pre-existing in the active region had participated in the eruption. The RHESSI data indicate that the looptop source at the top of the first group of flare loops, which was seen in EUV, was located between the footpoint sources.

The radio data were obtained by HSOS in the time interval from 07:00 UT to 07:12 UT with a spectral resolution of 4 MHz and a cadence of 0.2 s. In the impulsive phase of the X-ray flare, the radio emission displayed four well defined burst enhancements. The first and second bursts were observed in the periods from 07:07:14–07:07:40 UT and 07:07:42–07:08:08 UT, in the frequency ranges of 1.1–1.2 GHz and 1.12–1.23 GHz, respectively. The other two following bursts in the period from 07:08:20–07:12:00 UT displayed clear structures of a zebra pattern, and have been studied in detail by Huang et al. (2007) and Yan et al. (2010).

3 DATA ANALYSIS AND DISCUSSIONS

Figure 4 displays the dynamic spectrum of the burst. The three panels show the left and right circular polarization, as well as the polarization degree $p = (I_{\rm L} - I_{\rm R})/(I_{\rm L} + I_{\rm R})$. This burst showed weak polarization, indicating that the magnetic field in the source region is weak. Low polarization is also typical for harmonic plasma emission. A distinctive feature of the spectrum is the well organized narrow-band emission stripes. Their frequency drift indicates a successive pattern of motions in the source region. Such motions have often been reported to occur in the flare current sheet, both in observations (see Ko et al. 2003; Lin et al. 2005; Savage et al. 2010; Liu et al. 2010; Takasao et al. 2012) and in numerical experiments (Kliem et al. 2000; Shen et al. 2011; Bárta et al. 2011; and references therein). We classify these fine structures into three groups such that the stripes in each group display the same frequency drift characteristics.

The first group includes eight stripes in the low-frequency range with a positive frequency drift, ranging from 7 to 16 MHz s^{-1} (see stripes 1 through 8 in the upper panel of Fig. 4). The second group includes only one stripe in the high-frequency range (stripe 9) with a negative frequency drift, -2.37 MHz s^{-1}; and the third group includes eight stripes at intermediate frequencies (stripes 10 through 17) with approximately zero frequency drift. We re-draw these signal patterns in Figure 5 for clarity, and look into the detailed physics behind the various features in the following sections.

3.1 Electron Density Model used for Studying the Dynamic Spectrum

Plasma emission is the typical emission mechanism in the decimetric range, especially if narrow-band fine structures are present (e.g., McLean & Labrum 1985). This process relates the emission
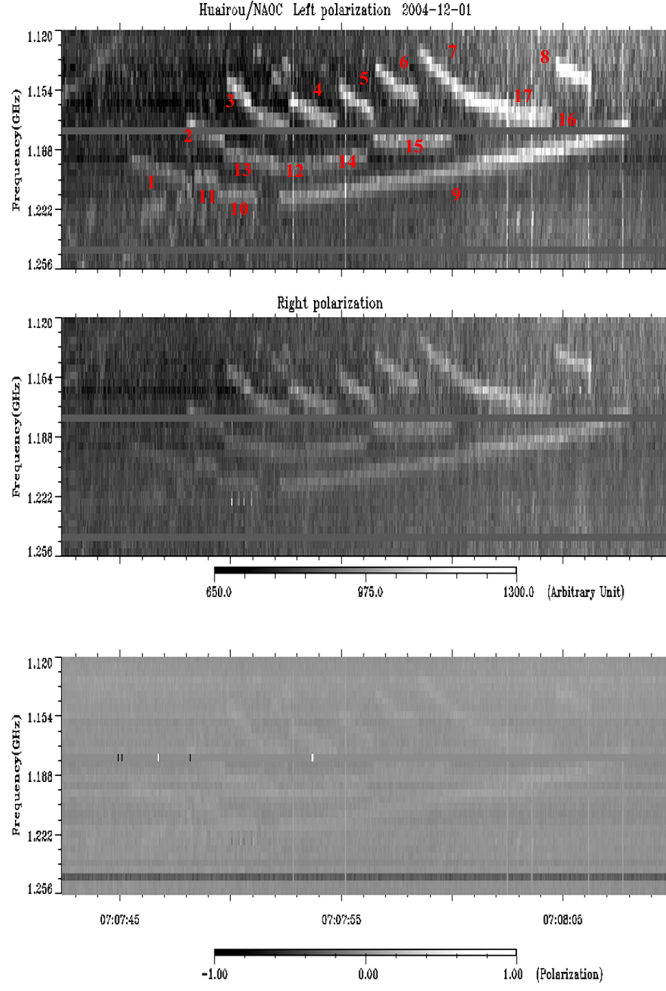
Fig. 4 Dynamic spectrum of the event obtained in the frequency range $1.12-1.226$ GHz from 07:07:42 UT to 07:08:08 UT. From top to bottom: left-circularly polarized flux I_{L}; right-circularly polarized flux I_{R}, and polarization degree $p = (I_{\mathrm{L}} - I_{\mathrm{R}})/(I_{\mathrm{L}} + I_{\mathrm{R}})$. The color bar below the second panel specifies the flux in arbitrary units, and that at the bottom specifies the polarization degree.

frequency f_{obs} to the electron plasma frequency f_{p} and electron number density n_{e} in the burst source region by

$$f_{\mathrm{obs}} = s f_{\mathrm{p}}, \quad f_{\mathrm{p}} = 8.98 \times 10^{-3} \sqrt{n_{\mathrm{e}}} \ (\mathrm{MHz}). \tag{1}$$

The harmonic number s here is either for fundamental ($s = 1$) or for harmonic ($s = 2$) plasma emission. Using a coronal density model, the emission frequency can thus be mapped to a height in the corona, and the frequency drift yields the velocity of a moving source. Since we cannot unambiguously associate the stripes with either the fundamental (F) or harmonic (H) emission (no F-H pattern is apparent), we perform the analysis for both assumptions, $s = 1$ and $s = 2$.
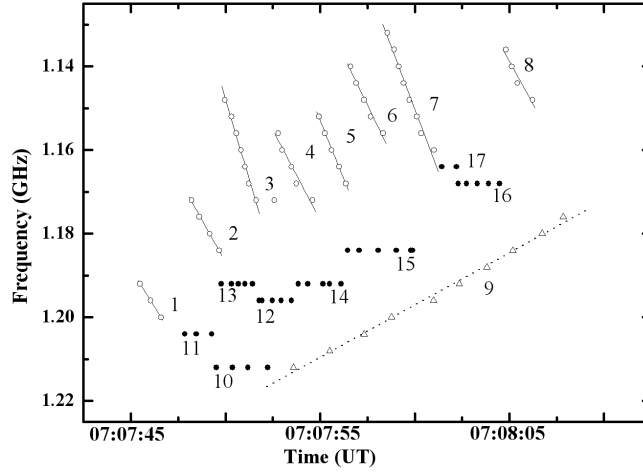
Fig. 5 A dot-and-time version of the dynamic spectrum displayed in the upper panel of Fig. 4. Open circles are for the signals with positive frequency drift, solid ones are for those of zero frequency drift, and triangles are for negative drift. This event contains positively and negatively drifting stripes, with linear fits yielding drift rates for stripes 1 to 9 of 7.23, 8.08, 15.3, 8.61, 11.2, 9.37, 12, 8.22 and -2.37 MHz s^{-1}, respectively.

In this work, we choose the density model of Aschwanden & Benz (1995)

$$n_{\mathrm{e}}(h) = \begin{cases} n_1 (h/h_1)^{-p} & h < h_1, \\ n_{\mathrm{Q}} \exp(-h/\lambda) & h > h_1, \end{cases} \tag{2}$$

where h_1 is a transition height at which the way n_{e} changes depends on h. This model is constrained by the electron density n_{Q} at the base of the quiet corona and the density scale height λ. A smooth transition between the two regimes is obtained by requiring that the function and its first derivative be continuous at the transition height $h = h_1$, which yields

$$h_1 = p\lambda, \quad n_1 = n_{\mathrm{Q}} \exp(-p), \tag{3}$$

with $p = 2.38$, $\lambda = 6.9 \times 10^4$ km and $n_{\mathrm{Q}} = 4.6 \times 10^8$ cm^{-3}. This model was developed for the region that has been affected by the flare process, and is thus appropriate for the case studied here.

3.2 Interpretation of the Fine Structure

From Equations (1) and (2), a positive (negative) frequency drift signifies sunward (anti-sunward) motion of the source, and we ascribe the positive drifting stripes to the trajectories of plasma blobs (magnetic islands) that were produced by magnetic reconnection in the flare current sheet. Figure 6(a) plots the heights of each sunward moving blob, converted from Figure 5 according to Equations (1) and (2), and the corresponding velocity deduced for each blob is listed in Table 1. We see these blobs moving at speeds ranging from 66 to 148 km s^{-1} for fundamental emission or from 118 to 265 km s^{-1} for harmonic emission.

The negative drift of stripe 9 corresponds to a slow upward motion of the source at a speed of 23 km s^{-1} for fundamental emission and 41 km s^{-1} for harmonic emission (Fig. 6(b)). Based on
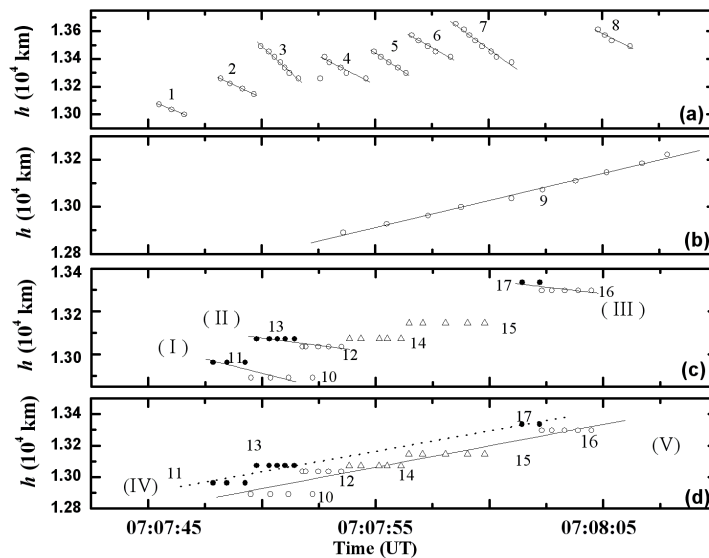
Fig. 6 The inferred source heights, with linear fits to the source motion overlaid, for (a) the positively drifting stripes 1–8, (b) the negatively drifting stripe 9, (c) the stationary stripes 10–17 showing groups I–III, and (d) the stationary stripes showing groups IV–V (as defined in the text). Speeds derived from linear fits for each group are overlaid.

this velocity, we suggest that stripe 9 resulted from the gradual ascent of the flare loop system in the event.

Different from stripes 1 through 9, stripes 10 through 17 do not indicate any motion. Instead they are basically from approximately stationary signals that imply no source motion (see the open and closed circles as well as triangles in Figures 6(c) and 6(d)). According to the standard model of the two-ribbon flare (Fig. 1), a TS on the flare loop top scenario could be considered responsible for this phenomenon (e.g., see also Aurass et al. 2002 and Aurass & Mann 2004) although occurrence and direct observations of TS are still an open question.

We recognize that our data exhibit more features that can be related to the consequences of re-connection in the flare current sheet. One can group stripes 10–17 in two different ways which reveal two patterns of frequency shift within the groups, although the individual elements are stationary. Looking into the relative locations suggested by stripes 10 through 13, and stripes 16 and 17, we see a pattern of decreasing heights from locations 11 to 10, from 13 to 12 and from 17 to 16 (see Fig. 6(c)), as well as the fact that the higher the altitude, the smaller the change is in altitude. We suggest that the data in these three pairs describe the descending motion of flare loops, and we mark them as I–III respectively. The corresponding velocities are listed in Table 2, where the minus sign indicates sunward displacement. In addition, stripes 11, 13 and 17, and stripes 10, 12, 14 through 16 constitute another two groups, namely groups IV and V respectively, which describe an upward motion scenario. The corresponding velocities are also listed in Table 2.

According to previous works by Svestka et al. (1987); Lin et al. (1995); Forbes & Acton (1996); Hiei & Hundhausen (1996) and Lin & Soon (2004), we explain such a combination as the shrinkage of individual loops which relax after their field lines were reconnected (groups I through III), and the growth of the flare loop system due to the accumulation of the same reconnected field lines (groups

Table 1 Results of the analysis of the radio bursts. Estimated values of the source parameters: frequency drift rate (df/dt), initial position of the source (H_i) and emission source velocity (v_b). Values in parentheses represent the estimations for harmonic emission.

Stripe	df/dt (MHz s^{-1})	H_i (10^4 km)	v_b (km s^{-1})
1	7.23	1.31 (2.34)	−66 (−118)
2	8.08	1.33 (2.37)	−76 (−136)
3	15.3	1.35 (2.42)	−148 (−265)
4	8.61	1.34 (2.40)	−83 (−148)
5	11.2	1.35 (2.41)	−108 (−194)
6	9.37	1.36 (2.43)	−92 (−166)
7	12	1.37 (2.44)	−118 (−211)
8	8.22	1.36 (2.44)	−82 (−147)
9	−2.37	1.29 (2.31)	23 (41)

Notes: '−' means the sources of emission are moving sunward.

Table 2 Estimated values of the source parameters: emission source velocity (v_l); values in parentheses represent the estimations for harmonic emission.

Marker	Stripe	v_l (km s^{-1})
I	11, 10	−26.7 (−36)
II	13, 12	−13.8 (−24.7)
III	17, 16	−12.5 (−22.4)
IV	11, 13, 17	26.1 (46.7)
V	10, 12, 14, 15, 16	27.2 (48.8)

Notes: '−' means the sources of emission are moving sunward.

IV and V). Figure 7, which is duplicated from Lin (2004), demonstrates how flare loops behave, and how the theoretical results could be related to the observational ones.

Considering the morphology of the dynamic spectrum, we found that the stripes studied here are quantitatively different from the radio signatures of the chromospheric evaporation observed by Aschwanden & Benz (1995). First, the velocities of stripes 1 to 8 are lower than the typical speed of the type III radio burst exciter (e.g. 0.1–0.3 c as shown in Aschwanden & Benz 1995) by several orders of magnitude. Second, the negative frequency drifting rate of stripe 9 is about –2 MHz s^{-1}, and is similar to that associated with the chromospheric evaporation reported by Ning et al. (2009). However, the drift rate here was much lower than the average one (46.4 ± 28.0 MHz s^{-1}) as suggested by Aschwanden & Benz (1995). Furthermore, from the RHESSI image, the transient X-ray source appeared at 07:08:00 UT and then disappeared 20 s later (see fig. 5 in Ning et al. 2009), which is apparently shorter than the timescale (about 1 min) of the typical chromospheric evaporation observed in hard X-rays (Liu et al. 2006).

In addition, the radio fine structures in Figure 4 are quasi-periodic, the time interval of the occurrence of the sunward plasmoids structures in Figure 4 is ∼2 s and their frequency drift as a motion of the waves (such as Alfvén wave, turbulent flow, etc) modulates the radio emission as a result of the plasma emission (Huang et al. 2003). From the slowly-drifting highest-frequency case of stripe 9, we estimate the height of the flare loop arcade to be about 13 000 km (F) or 23 000 km (H). This is consistent with the height indicated by the footpoint separation of ≈ 29 000 km seen in the EUV and X-ray images if the shape of a semicircular loop is assumed.

The radio burst observed here also gave us a good opportunity to study the process of the magnetic reconnection outflow. Below the zero-drift stripes, which in our interpretation indicates the position of the TS, stripe 9 with negative drift rate exists. We suggest that this stripe resulted from
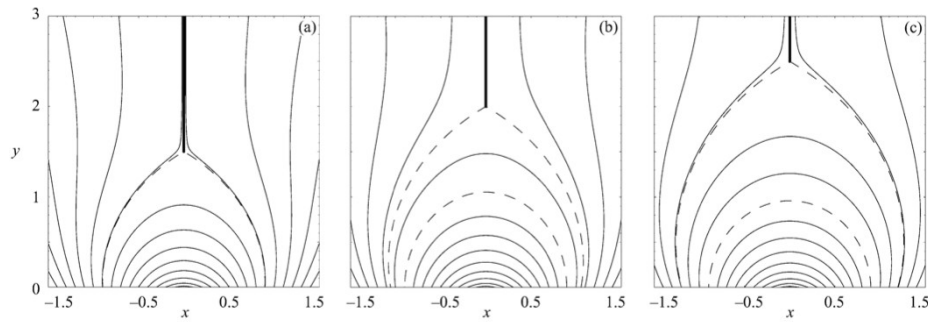
Fig. 7 Schematic demonstration of how a specific field line shrinks after it is closed as a result of reconnection and becomes detached from the current sheet that is denoted with the *thick solid lines*. This field line is denoted by one dashed curve. Another dashed curve that is always attached to the current sheet traces the separatrix. (a) At time t_1, when this field line is attached to the current sheet, it is the instant separatrix. (b) At time t_2, it leaves the current sheet, shrinks to a lower altitude, and the separatrix moves to another field line, when the flare loop system expands outward. (c) At time t_3, this field line keeps shrinking, the separatrix moves further to the new field line, and the flare loop system keeps expanding further (from Lin 2004).

the downstream region of the TS where the growing flare loops occur, which consist of successively formed new loops. The corresponding velocity inferred from the drift rate is comparable to the group-based displacement velocity of the zero-drift stripes in groups IV and V (see Fig. 6(d) and Table 2), and it lies in the range of velocity obtained from studies of the other events (Khan et al. 2006, 2007; Romano et al. 2009; Yan et al. 2013). We note that the upward motion of the source in stripe 9 cannot come from an anti-sunward moving plasma blob, because such a blob could not penetrate the newly reconnected field lines carried downward by the reconnection outflow.

4 CONCLUSIONS

The solar radio burst presented in the 2004 December 1 event in the 1.12–1.23 GHz band displayed interesting spectral fine structures in the form of the narrow-band stripes with a systematic drift pattern, which allows us to look into the dynamics of the reconnection process in flares.

We propose an interpretation in terms of plasmoid dynamics in the reconnecting flare current sheet and the underlying flare loop arcade. The stripes in the low-frequency part of the band exhibited positive frequency drift that was high initially but decreased to a drift rate of nearly zero. They are believed to trace plasmoids in the downward reconnection outflow. The stripe in the high-frequency part of the band showed a long-lasting small negative frequency drift. This is interpreted as a radio source at the top of the growing flare loop arcade which was always associated with the highest (most newly formed) loops by reconnection, which were filled with energetic particles. Stripes with zero frequency drift were located between the two groups, which implies the occurrence of the TS on the top of the flare loops, although this issue is still an open question.

From the slowly-drifting highest-frequency stripe, we estimated the height of the flare loop arcade to be about 13 000 km (F) or 23 000 km (H). By grouping the zero-frequency stripes in three pairs (groups I–III), we found evidence of the shrinkage of the flare loop in the process of their relaxation in the top part of the arcade, and the shrinking velocities that were deduced lie in the range 13–27 km s^{-1} (F) and 22–36 km s^{-1} (H).

The relatively low polarization degree of less than 25% favors harmonic emission. However, it could also result from low field strength in the reconnection outflow region. The inferred height and velocity data appear consistent with both F and H emissions, with a slightly better match of the

inferred downward plasmoid of supra-arcade downflows in the impulsive phase of the flare studied here (see also Asai et al. 2004) for H emission.

Plasma emission is good for diagnosing the dynamics and properties of the flaring plasma. The spectral fine structures of the investigated event show a clear organization which allowed us to comprehensively study the formation of plasmoids and their evolution in the flare current sheet, their interaction with the flare loops and the growth of the flare loop arcade associated with the shrinkage of individual flare loops in the impulsive flare phase.

References

Asai, A., Yokoyama, T., Shimojo, M., & Shibata, K. 2004, ApJ, 605, L77

Aschwanden, M. J., & Benz, A. O. 1995, ApJ, 438, 997

Aurass, H., Vršnak, B., & Mann, G. 2002, A&A, 384, 273

Aurass, H., & Mann, G. 2004, ApJ, 615, 526

Bárta, M., Büchner, J., Karlický, M., & Skála, J. 2011, ApJ, 737, 24

Brueckner, G. E., Howard, R. A., Koomen, M. J., et al. 1995, Sol. Phys., 162, 357

Delaboudinière, J.-P., Artzner, G. E., Brunaud, J., et al. 1995, Sol. Phys., 162, 291

Forbes, T. G., & Acton, L. W. 1996, ApJ, 459, 330

Fu, Q., Qin, Z., Ji, H., & Pei, L. 1995, Sol. Phys., 160, 97

Fu, Q., Ji, H., Qin, Z., et al. 2004, Sol. Phys., 222, 167

Hiei, E., & Hundhausen, A. J. 1996, in IAU Colloq. 153, Magnetodynamic Phenomena in the Solar Atmosphere - Prototypes of Stellar Magnetic Activity, eds. Y. Uchida, T. Kosugi, & H. S. Hudson 125 (Dordrecht: Kluwer Academic Publishers)

Hill, S. M., Pizzo, V. J., Balch, C. C., et al. 2005, Sol. Phys., 226, 255

Huang, G. L., Wu, H. A., Grechnev, V. V., Sych, R. A., & Altyntsev, A. T. 2003, Sol. Phys., 213, 341

Huang, G., & Lin, J. 2006, ApJ, 639, L99

Huang, J., Yan, Y., & Liu, Y. 2007, Advances in Space Research, 39, 1439

Karlický, M., & Bárta, M. 2012, in Astronomical Society of the Pacific Conference Series, 454, Hinode-3: The 3rd Hinode Science Meeting, eds. T. Sekii, T. Watanabe, & T. Sakurai, 287

Khan, J. I., Fletcher, L., & Nitta, N. V. 2006, A&A, 453, 335

Khan, J. I., Bain, H. M., & Fletcher, L. 2007, A&A, 475, 333

Kliem, B., Karlický, M., & Benz, A. O. 2000, A&A, 360, 715

Ko, Y.-K., Raymond, J. C., Lin, J., et al. 2003, ApJ, 594, 1068

Lin, J., Forbes, T. G., Priest, E. R., & Bungey, T. N. 1995, Sol. Phys., 159, 275

Lin, J., & Forbes, T. G. 2000, J. Geophys. Res., 105, 2375

Lin, R. P., Dennis, B. R., Hurford, G. J., et al. 2002, Sol. Phys., 210, 3

Lin, J., Soon, W., & Baliunas, S. L. 2003, New Astron. Rev., 47, 53

Lin, J. 2004, Sol. Phys., 222, 115

Lin, J., Raymond, J. C., & van Ballegooijen, A. A. 2004, ApJ, 602, 422

Lin, J., & Soon, W. 2004, New Astron., 9, 611

Lin, J., Ko, Y.-K., Sui, L., et al. 2005, ApJ, 622, 1251

Liu, W., Liu, S., Jiang, Y. W., & Petrosian, V. 2006, ApJ, 649, 1124

Liu, R., Lee, J., Wang, T., et al. 2010, ApJ, 723, L28

Mann, G., Aurass, H., & Warmuth, A. 2006, A&A, 454, 969

McLean, D. J., & Labrum, N. R. 1985, Solar Radiophysics - Studies of Emission from the Sun at Metre Wavelengths (Cambridge: Cambridge Univ. Press)

Ning, Z., Cao, W., Huang, J., et al. 2009, ApJ, 699, 15

Romano, P., Zuccarello, F., Fletcher, L., et al. 2009, A&A, 498, 901

Savage, S. L., McKenzie, D. E., Reeves, K. K., Forbes, T. G., & Longcope, D. W. 2010, ApJ, 722, 329

Shen, C., Lin, J., & Murphy, N. A. 2011, ApJ, 737, 14

Svestka, Z. F., Fontenla, J. M., Machado, M. E., Martin, S. F., & Neidig, D. F. 1987, Sol. Phys., 108, 237

Takasao, S., Asai, A., Isobe, H., & Shibata, K. 2012, ApJ, 745, L6

Yan, X. L., Pan, G. M., Liu, J. H., et al. 2013, AJ, 145, 153

Yan, Y., Huang, J., Chen, B., Liu, Y., & Tan, C. 2010, Advances in Space Research, 46, 413